Organic & Biomolecular Chemistry

PAPER

View Article Online
View Journal

CrossMark click for updates

Cite this: DOI: 10.1039/c5ob00704f

The synthesis of new fluorescent bichromophoric compounds as ratiometric pH probes for intracellular measurements†

A. Vanessa Saura,[a] María J. Marín,[b] M. Isabel Burguete,[a] David A. Russell,[b] Francisco Galindo*[a] and Santiago V. Luis*[a]

Received 8th April 2015,
Accepted 8th June 2015

DOI: 10.1039/c5ob00704f

www.rsc.org/obc

Three different bichromophoric compounds (**1–3**) containing an aminomethyl anthracene moiety linked to a second chromophore (pyrene, 4-nitrobenzo-2-oxa-1,3-diazole (NBD) and dansyl) through a valine-derived pseudopeptidic spacer have been prepared and their fluorescent properties studied. The results obtained show that upon irradiation the photophysical behavior of these probes involves electronic energy transfer from the excited anthracene to the second chromophore and also intramolecular photoinduced electron transfer. The X-ray structure obtained for **3** reveals that the folding associated with the pseudopeptidic spacer favours a close proximity of the two chromophores. The emissive response of **3** is clearly dependent on the pH of the medium, hence this bichromophoric compound was shown to be an excellent ratiometric pH fluorescent sensor. The emission intensity due to the anthracene moiety exhibits a decrease at neutral–basic pH values that is concomitant with an increase in the intensity arising from the dansyl fluorophore. These properties make this compound a good candidate for biological pH sensing as has been confirmed by preliminary studies with RAW 264.7 macrophage cells imaged by means of confocal fluorescence microscopy with an average pH estimation of 5.4–5.8 for acidic organelles.

Published on 19 June 2015. Downloaded by Freie Universitaet Berlin on 02/07/2015 14:49:49.

Introduction

Chemical fluorescence sensing[1] is currently used as a powerful tool in biomedical applications including the study of fundamental processes at the intracellular level.[1,2] Many efforts have been devoted to the development of efficient fluorescent sensors for the measurement of pH.[3] Fluorescent pH sensors can be classified according to several criteria, for example: the pH range of application (for neutral-alkaline or for acidic environments); the spectral features of the probes (*i.e.* UV, visible or NIR excitation) or the chemical nature of the pH-sensitive systems (aromatic polycyclic compounds, lanthanide complexes and metallic nanoparticles among others). Fluorescent pH sensors can also be classified according to the mechanism that explains their sensitivity towards protons. In this regard, the phenomenon of photoinduced electron transfer (PET) has been exhaustively used to develop pH probes as well as other chemosensing systems.[4] Under neutral conditions, the electron transfer process that operates in PET probes quenches the emission from the fluorophore, due normally to the presence of a close free amine group capable of charge transfer to an electron-deficient excited moiety. In such systems, the protonation of the amine in acidic medium leads to disruption of the PET process and hence restoration of the emission from the excited fluorophore occurs. For probes relying on the PET mechanism, the lower the pH of the medium the higher the fluorescence intensity displayed.[5,6] This behavior is in sharp contrast to the one observed for other families of fluorescent pH probes, for which the fluorescence intensity increases with an increase of the pH of the medium. Examples of this second type of pH sensor are systems based on fluorescein derivatives where the switching mechanism is based mainly on the phenol–phenolate equilibrium, affording a more emissive species at basic–neutral pH, where the phenolate form prevails, than at acidic pH.[7] Hence,

[a]*Departamento de Química Inorgánica y Orgánica, Universitat Jaume I, Campus del Riu Sec, Av. Sos Baynat, s/n, E-12071 Castellón, Spain.*
E-mail: francisco.galindo@uji.es, luiss@uji.es
[b]*School of Chemistry, University of East Anglia, Norwich Research Park, Norwich, Norfolk NR4 7TJ, UK*

†Electronic supplementary information (ESI) available: ^{1}H and ^{13}C-NMR and mass spectra of bichromophoric compounds **1–3** and model compounds **9–10**; absorption spectra of compounds **1–3**; absorption and emission spectra of models **9–10**; fluorescence pH titration spectra and titration curves of **9** and **10**; NMR analysis of structural features of **3**, **9** and **10**; X-ray crystallographic analysis for **3**; distribution and fluorescence emission spectra of bichromophoric compound **3** in RAW 264.7 macrophage cells. CCDC 1057020. For ESI and crystallographic data in CIF or other electronic format see DOI: 10.1039/c5ob00704f

Published on 19 June 2015. Downloaded by Freie Universitaet Berlin on 02/07/2015 14:49:49.

according to the previously described behavior, two types of pH titration curves can be found: *S-shaped* titration curves, more emissive at higher pH values (typical behavior of fluoresceins) and *Z-shaped* titration curves, more emissive at lower pH values (typically found with PET probes).

In this paper we describe a new pH probe with a large pseudo-Stokes shift operating *via* the well-known PET mechanism for which, remarkably, the emission at neutral–basic conditions is higher than that at acidic pH, hence displaying an S-shaped titration curve. This behavior has been accomplished by the appropriate combination of two fluorophores (anthracene and dansyl) linked by a flexible spacer yielding compound **3**. Despite the apparent simplicity of the bichromophoric probe, the appropriate selection of the emitting moieties is the key factor for the success of the sensor. Other assayed combinations, such as anthracene with either pyrene (compound **1**) or 4-nitrobenzo-2-oxa-1,3-diazole (NBD, compound **2**) failed to afford pH probes exhibiting this behavior. At the mechanistic level, the results are described as a combination of electronic energy transfer (EET) from the excited anthracene moiety to the dansyl fragment along with a competitive PET process. Additionally, the bichromophoric compound displays a large pseudo-Stokes shift, which is valuable for biological applications since excitation and emission are separated to avoid self-absorption phenomena or autofluorescence. Compound **3** was used to perform intracellular measurements within RAW 264.7 mouse macrophage cells. The confocal fluorescence images and the fluorescence emission spectra of the bichromophoric compound **3** from within the RAW 264.7 cells confirmed the internalization of the probe by the cells. Co-localization experiments were performed using LysoTracker Red DND-99 as a marker of acidic organelles. Compound **3** was distributed around the cell with partial localization in the organelles marked by the DND-99, probably marking early and late endosomes within the treated RAW 264.7 cells.

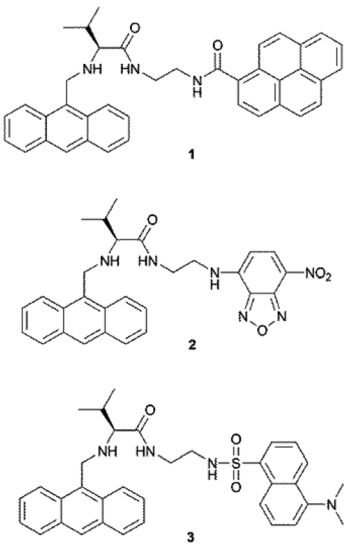

Chart 1 Structures of compounds **1–3**.

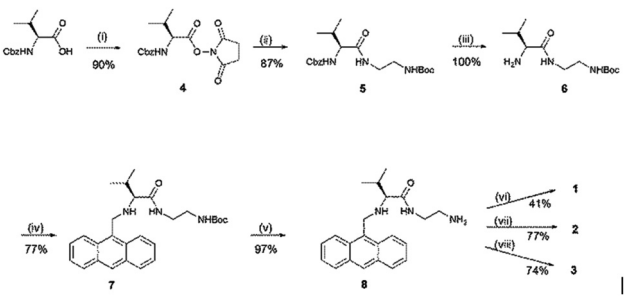

Scheme 1 Synthesis of compounds **1–3**. (i) NHS, DCC, THF. (ii) *N*-Boc-ethylenediamine, THF. (iii) Pd/C, H_2, MeOH. (iv) 9-(Chloromethyl)anthracene, K_2CO_3, TBAI, CH_3CN. (v) HCl, MeOH. (vi) 1-Pyrenecarboxylic acid, $SOCl_2$, Et_3N, CH_2Cl_2. (vii) NBD-Cl, EtOH. (viii) DNS-Cl, Et_3N, CH_2Cl_2.

Results and discussion

Synthesis and characterization

The bichromophoric compounds **1–3** shown in Chart 1 were designed as potential pH probes displaying interchromophoric communication. Compounds **1–3** were synthesized starting from *N*-protected amino acid valine, which was activated at the carboxyl group using *N*-hydroxysuccinimide (NHS)/*N*,*N*′-dicyclohexylcarbodiimide (DCC) chemistry.[8] The activated amino acid was further reacted with ethylenediamine (Boc-monoprotected) to give **5**. After deprotection of the Cbz group and reaction with 9-(chloromethyl)anthracene, compound **7** was obtained, which was deprotected in acidic medium to afford amine **8**. This intermediate was used as a common building block for the synthesis of the target probes (**1–3**) by reaction with 1-pyrenecarboxylic acid (to obtain **1**), with NBD-Cl (to afford **2**) and with dansyl chloride (to yield **3**), as indicated in Scheme 1. The compounds were characterized by $^1H/^{13}C$-NMR, high resolution mass spectrometry (HRMS) and IR spectroscopy confirming the structures depicted in Chart 1 (see ESI, Fig. S1–S3†). Moreover, compound **3** afforded a crystal suitable for X-ray diffraction (Fig. 1).

The main features of the X-ray structure obtained for compound **3** are presented in Fig. 1. The presence of an intramolecular hydrogen bond between the hydrogen atom of the amide group and the nitrogen of the amino functionality facilitates a folding of the structure that allows an almost perpendicular arrangement (84° dihedral angle) of the two aromatic rings at a short distance. This intramolecular H-bond is common to many related pseudopeptidic compounds and often defines their final conformational and structural arrangements observed both in the solid state and in solution.[8,9] An intramolecular offset edge-to-face geometry is adopted by the aromatic rings, with two H-atoms of one of the anthracene rings located at about 3 Å from the closest carbon atoms of the naphthalene from the dansyl moiety. An almost perfect edge-to-edge geometrical configuration is observed,

 This journal is © The Royal Society of Chemistry 2015

Published on 19 June 2015. Downloaded by Freie Universitaet Berlin on 02/07/2015 14:49:49.

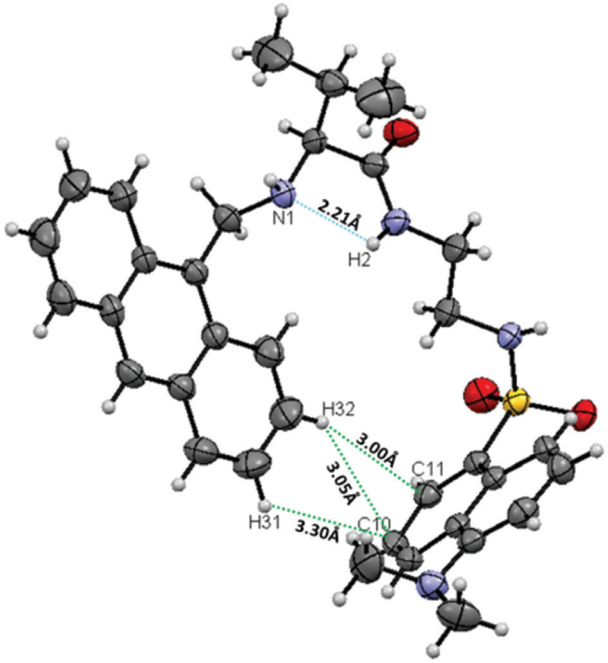

Fig. 1 ORTEP plot of the crystal structure of bichromophoric compound **3** showing an intramolecular H-bond between the hydrogen atom of the amide group and the nitrogen of the amino functionality, which facilitates the occurrence of a folded conformation approaching the two fluorophores, and some of the possible C–H···π interactions between anthracene (CH) and dansyl (π).

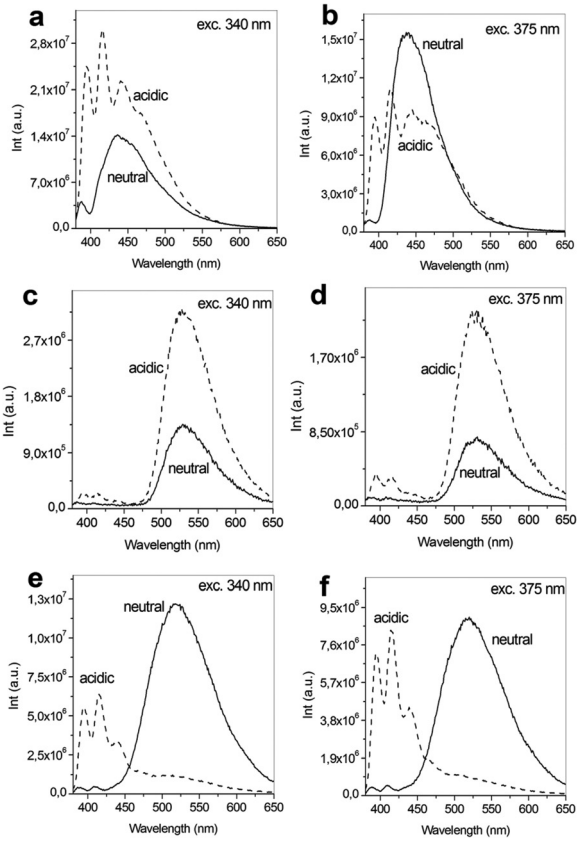

Fig. 2 Fluorescence emission spectra of the studied compounds in MeOH (—) and MeOH with addition of an excess of trifluoroacetic acid (---): (a and b) bichromophoric compound **1** (3.8×10^{-5} M); (c and d) bichromophoric compound **2** (5.3×10^{-5} M); (e and f) bichromophoric compound **3** (3.9×10^{-5} M). Excitation wavelengths: 340 nm (a, c and e) and 375 nm (b, d and f).

displaying the following parameters: H32···C11 = 3.00 Å, H32···C10 = 3.05 Å, H31···C10 = 3.30 Å and H31···C9 = 3.26 Å, representing values of $\%vdW_{H,C}$ of 101.0, 102.7, 111.1 and 109.8, respectively ($\%vdW_{H,C}$ is calculated, for a given measured distance, as the percentage of the sum of the van der Waals radii of H and C: 1.20 + 1.77 = 2.97 Å).[10] The distance between the centroids of the closest rings is 5.14 Å. It should be noted that a $\%vdW_{H,C}$ value of 100 is by no means the outer limit of an attractive interaction.[11] The $\%vdW_{H,C}$ values obtained for the above mentioned pairs of H–C in the structure of **3** are consistent with the range considered by Alvarez for atoms placed at appropriate distances to be likely to establish van der Waals interactions.[10]

Spectroscopic studies

The absorption and fluorescence emission spectra of the three bichromophoric compounds were recorded in methanolic and acidic methanol media (see Fig. S6† for the absorption spectra and Fig. 2 for the fluorescence emission spectra).

The fluorescence emission spectrum of the anthracene–pyrene bichromophoric compound **1** in neutral medium exhibits a broad band centered at *ca.* 440 nm when exciting at either λ = 340 nm (Fig. 2a) or λ = 375 nm (Fig. 2b). These spectral bands are coincident with neither the typical emission spectrum of anthracene (vibrationally structured emission between 400 and 500 nm) nor that of pyrene (structured emission between 370 and 450 nm).[12] The formation of an exciplex between the two chromophores could explain the shape of the emission spectrum.[13] Desvergne *et al.* have described this phenomenon in related anthracene and pyrene dyads,[14] which was later used by Zhou *et al.* to design probes for micellization.[15] However, not all the systems containing anthracene and pyrene form exciplexes between the two chromophores. For example, Campagna *et al.* have described compounds containing anthracene and pyrene moieties that only exhibit the emission features of the anthracenyl component, pointing to an electronic energy transfer (EET) process from pyrene to anthracene.[16] This process could account for the behavior of **1** under acidic conditions (see Fig. 2a and b, dashed lines). The fluorescence emission spectra under acidic and neutral conditions, although having different shapes, are to a great extent coincident in position, hence molecule **1** is not able to distinguish between acidic and neutral environments, and therefore will not be further discussed in this work.

The fluorescence emission spectrum of the anthracene–NBD bichromophoric compound **2** in neutral methanol, upon excitation of the anthracene moiety, is dominated by an intense band centered at *ca.* 530 nm which can be attributed to the NBD chromophore (Fig. 2c and d, solid line).[17] The

Published on 19 June 2015. Downloaded by Freie Universitaet Berlin on 02/07/2015 14:49:49.

almost complete absence of emission below 450 nm suggests an efficient energy transfer process from the anthracenic substructure to the benzofurazan part of the bichromophoric compound. Samanta *et al.* have described an anthracene–NBD probe for transition metal ions in which PET from a secondary amine and EET between chromophores explain the observed spectral variations.[18] Assuming that both PET and EET are operating in compound **2**, the emission at 500–600 nm could be ascribed to an analogous EET process; however, it is not possible to clearly attribute the quenching of the anthracene emission uniquely to such a process or to its combination with the intramolecular PET from the proximal secondary amine. Under acidic conditions, *i.e.* when the amine is protonated and hence the PET process is blocked, the fluorescence emission from both excited fluorophores is enhanced, although to a different extent (Fig. 2c and d, dashed line). This compound displays a large pseudo-Stokes shift (the emission comes mainly from the NDB part of the molecule irrespective of the acidity of the medium) however, the differences in intensity between the protonated and unprotonated forms are not significant enough for the efficient use of compound **2** as a pH probe for biological applications.

Compound **3**, combining anthracene and dansyl chromophores, showed more interesting features as an acidity probe. The emission of the bichromophoric compound **3** in neutral methanol is dominated by a strong and broad band at 450–650 nm, due to the dansyl moiety (Fig. 2e and f, solid line). A weak emission of the anthracenic part of the probe is also appreciable at shorter wavelengths.[19] The attenuation of the anthracene fluorescence, together with the presence of the dansyl emission, suggests the existence of an energy transfer process from the anthracene moiety to the dansyl group in agreement with the reported description of such phenomena in other systems. For example, analogous processes have been observed for supramolecular complexes of dansylated hosts with anthracenic guests,[20] as well as in a dyad recently described by Kumar *et al.*[21] Compound **3** in an acidic medium displays a typical anthracenic fluorescence emission mainly centred at 400–450 nm, whereas the emission of the dansyl group is almost absent (Fig. 2e and f, dashed line).

For compound **3**, the emission at longer wavelengths could be explained by postulating the existence of an EET between the anthracene and the dansyl units (see Fig. 3). The EET process competes with a PET process from the amine close to the anthracene group which would also attenuate the emission from the anthracene part under neutral conditions (but not enough to prevent EET to the dansyl unit). An additional process that could occur is the PET from the excited anthracene unit to the dansyl fragment and *vice versa*. Pischel *et al.* have described in great detail dyads in which EET and combinations of PET processes take place and where the appropriate input can modulate the spectral behavior.[22] In order to gain an insight regarding the possibility of electronic energy transfer in compound **3**, two model compounds containing only anthracene (**9**) and dansyl (**10**) chromophores were synthesized and characterized (see Chart 2 for the chemical structure and

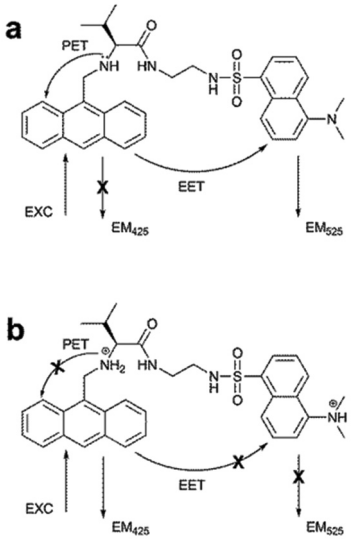

Fig. 3 Schemes showing the possible intramolecular PET and EET processes competing in bichromophoric compound **3** depending on the pH of the media: (a) neutral medium, (b) acidic medium.

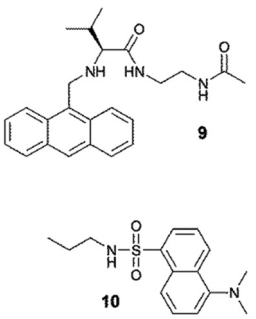

Chart 2 Structures of model compounds **9** and **10**.

Fig. S4, S5, S7 and S8† for the characterization). The photophysical features of **9** and **10** are shown in Table 1, along with those of **3**.

A basic requirement for the feasibility of EET is that the Gibbs free energy change should be negative. This value can be easily estimated using eqn (1):

$$\Delta G_{EET} = E_{S1}(10) - E_{S1}(9) \quad (1)$$

where E_{S1} is the singlet energy of the involved chromophores. Considering E_{S1} for dansyl as ~65 kcal mol^{-1} [23] and E_{S1} for 9-methylanthracene as ~73 kcal mol^{-1},[24] results in a favourable $\Delta G_{EET} = -8$ kcal mol^{-1}.

In Förster's theory,[12] the distance between the donor and the acceptor where the probability of an energy transfer process occurring is 50% is represented by R_0 and can be calculated using eqn (2), where ϕ_D is the fluorescence quantum yield of the donor in the absence of the acceptor, κ^2 is the orientation factor between the transition dipoles of the donor and acceptor (κ^2 = 2/3 assuming isotropical rotation of donor and acceptor), n is the average refractive index of the medium,

 This journal is © The Royal Society of Chemistry 2015

Published on 19 June 2015. Downloaded by Freie Universitaet Berlin on 02/07/2015 14:49:49.

Table 1 Photophysical characterization of the pH-sensitive compound **3** and its corresponding model compounds **9** and **10** in methanol

Comp.	Medium	Absorption[a] (λ, nm)	Emission[b] (λ, nm)	ϕ_F [c]	τ[d] (ns)
3	Neutral[e]	347, 365, 385	519	0.12	2.1 (73%), 8.6 (27%)
3	Acidic[f,g]	351, 369, 388	395, 415, 440	0.09	3.5
9	Neutral	347, 365, 385	389, 410, 435	0.06	7.3
9	Acidic[g]	351, 369, 388	395, 415, 440	0.35	7.5
10	Neutral	336	519	0.36	12.0
10	Acidic[g]	Weak tail <320 nm	Very weak	<0.01	Not measurable

[a] The absorption spectra were recorded over the range 190–600 nm. [b] The fluorescence emission spectra were recorded between 380 and 650 nm upon excitation at 375 nm. [c] Fluorescence quantum yield. [d] Fluorescence lifetime. [e] Emission from the dansyl part recorded; emission from anthracene moiety was too weak to be recorded. Dansyl moiety emission lifetime recorded at 550 nm. [f] Emission from the anthracene part recorded; emission from dansyl moiety was too weak to be recorded. Anthracene moiety emission lifetime recorded at 420 nm. [g] Excess of CF_3COOH added.

N_A is the Avogadro's number and J_{D-A} is the spectral overlap integral.

$$R_0^6 = \frac{9\ (\ln 10)}{128\pi^5 N_A}\frac{\kappa^2\phi_D}{n^4}J_{D-A} \quad (2)$$

Using the spectral features of **9** and **10**, the spectral overlap integral (J_{D-A}) between the emission of the donor (anthracene) and the absorption of the acceptor (dansyl), was calculated according to eqn (3):

$$J_{D-A} = \frac{\int_0^\infty F_D(\tilde{\nu})\varepsilon_A(\tilde{\nu})d\tilde{\nu}}{\tilde{\nu}^4} \quad (3)$$

In this equation, F_D represents the fluorescence of the donor in the absence of the acceptor and ε_A is the molar absorption coefficient of the acceptor at $\tilde{\nu}$.

The calculated overlap integral results in a value of J = 8.05386 × 10^{-13} cm^6 mol^{-1} and the Förster's distance calculated using eqn (2) is 14.4 Å, indicating that for distances shorter than 14.4 Å the probability of EET is >50%. From the X-ray structure of compound **3** (Fig. 1), an intramolecular distance of 7.70 Å between the two fluorophores was measured which suggests that the discussed EET is feasible.

The rate constants of such EET (k_{EET}) can be estimated according to eqn (4):

$$k_{EET} = \frac{1}{\tau_D}\left(\frac{R_0}{R}\right)^6 \quad (4)$$

where R is the estimated distance between chromophores and τ_D is the lifetime of the donor in the absence of the acceptor. When eqn (4) is employed to calculate the k_{EET} of compound **3** in neutral medium, using the X-ray data, a value of 6.0 × 10^{-9} s^{-1} can be expected from the theory.

The above mentioned considerations are based on the assumption that a dipole–dipole (Förster) mechanism operates in compound **3**. However, for interchromophoric distances shorter than 10 Å, the possibility of orbital overlap between chromophores is very high, hence leading to an EET *via* the exchange (Dexter) mechanism.

The complex pattern of fluorescence lifetimes in bichromophoric compound **3** as compared to the monoexponential behavior of model compounds **9** and **10** can be indicative of the multiple processes that take place when compound **3** is excited (see Table 1 for details). In addition, the analysis is complicated by the lack of data below the nanosecond timeframe from our set-up. To fully understand all of the photophysical processes of compound **3**, ultrafast data would be required.

The experimental EET efficiency can be calculated using eqn (5), where F_{DA} is the fluorescence emission intensity of the donor in the presence of the acceptor and F_D is the fluorescence emission intensity of the donor in the absence of the acceptor:

$$\Phi_{EET} = 1 - \frac{F_{DA}}{F_D} \quad (5)$$

An EET efficiency of 92% can be estimated from the fluorescence emission intensity of model **9** and of the bichromophoric compound **3** in a neutral medium (considering the anthracenic emission). However, the value would be valid only considering the existence of an EET process, which is not the case for compound **3** since a PET pathway yielding to deactivation of the anthracene singlet excited state is also possible. Thus, the system presented here can be considered as a bichromophoric compound exhibiting a mixed EET/PET behavior. Moreover, the emission of the dansyl chromophore in neutral medium should be also deactivated *after* the EET, since the calculated emission quantum yield of this moiety in compound **3** is 0.12, much lower than the ϕ = 0.36 recorded for the model compound **10**. Furthermore, additional deactivating processes must take place also in acidic conditions *after* the EET has occurred, since the maximum emission quantum yield measured from the anthracene part is 0.09, far from the value of 0.35 measured for the model compound **9** under identical conditions.

To further this study, we have concentrated on the potential applicability of compound **3** as a pH probe.

Acid–base titration of compound 3

The potential suitability of bichromophoric compound **3** for pH sensing in an aqueous environment was investigated. Fig. 4 shows the fluorescence emission spectrum of compound

Published on 19 June 2015. Downloaded by Freie Universitaet Berlin on 02/07/2015 14:49:49.

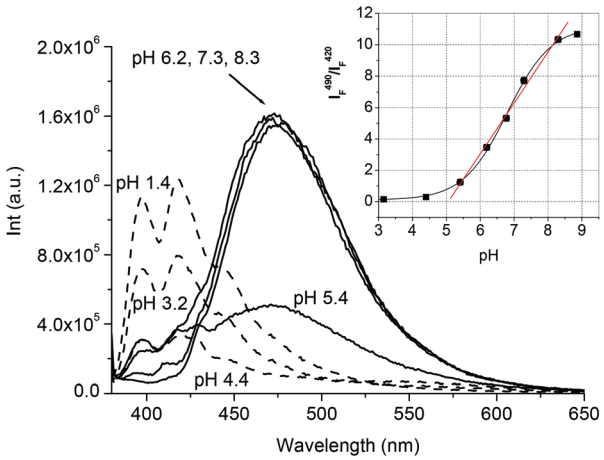

Fig. 4 Fluorescence titration of the anthracene–dansyl bichromophoric compound **3** as a function of the pH in aqueous solution (0.2% DMSO). The concentration of compound **3** was 2×10^{-6} M. NaCl was added at a concentration of 0.1 M. λ_{exc} = 375 nm. Inset: pH titration curve of **3** (representation of the ratio I^{490}/I^{420} *vs.* pH) and linear calibration allowing for ratiometric measurements of pH.

3 at different pH values. As anticipated from the preliminary measurements in methanol, the only fluorescence in the neutral–basic pH region is that arising from the dansyl chromophore, whereas in the acidic pH region, the prevalent emission is due to the anthracene chromophore. These results conclude that compound **3** is a dual fluorescence pH probe which is able to emit in two different spectral regions as a function of the pH of the medium thus enabling the possibility of ratiometric measurements.

The titration curve of compound **3** representing the ratio of intensities at 490 nm and 420 nm *vs.* pH (Fig. 4, inset) afforded an apparent pK_a of 5.6, which lies within the same range of other sensors bearing anthracene units linked to amino acid structures.[6] Moreover, it offers the possibility of quantifying the pH of the media in a range around neutrality.

Interestingly, the shape of the titration curve (S-shaped) is opposite to the standard titration curves described for amine-based PET probes (Z-shaped). This can be described by considering that a classical *on–off* probe (from acidic to neutral–basic pH) has been converted to an *off–on* probe for the same pH modification. The switching mechanism must rely on the protonation of the secondary amine proximate to the anthracene group since the pK_a of the model compound **9**, structurally similar to **3** but containing only the anthracene chromophore, was determined by fluorescence titration as 6.3 (see Fig. S12† for pH titration). The protonation of the dimethylamino group in the dansyl part of the molecule brings about a decrease in its emission. However, this occurs at much lower values of pH (pK_a ~ 3.5, an environment two orders of magnitude more acidic), as demonstrated by the pH titration of the model compound **10** (see Fig. S13† for pH titration).[25]

The fluorescence emission maximum of the dansyl chromophore of **3** in an aqueous solution (Fig. 4) is notably blue shifted, *ca.* 80 nm, with respect to its expected position in water. As described in the literature, the fluorescence emission maximum of dansylated compounds is strongly dependent on the polarity of the media. Dansylated model compounds are reported to have the following emission maxima:[26] 462 nm (cyclohexane), 506 nm (dichloromethane), 525 nm (methanol) and 559 nm (water). Hence, it seems remarkable that the emission band of compound **3** at neutral–basic pH is centered at *ca.* 476 nm. To explain the behavior exhibited by compound **3**, we can consider that compound **3** in water is expected to be folded, rendering a certain hydrophobic environment to the dansyl chromophore and therefore, reducing its complete solvation by water molecules. In fact, this folding and enhanced hydrophobicity would justify why the pK_a of the bichromophoric compound **3** is slightly lower than that of **9**. Folded conformations of pseudopeptidic molecules are common, involving important changes in the physical properties as previously demonstrated.[8,9,27] Hydrogen bonding or aromatic interactions similar to those observed in the X-ray structure of **3** are normally at the origin of such spatial orientations. This hypothesis is also supported by the description of other dansylated systems experiencing similar effects. For instance, the group of Corradini has described dansylated cyclodextrins whose emission is notably blue shifted due to the inclusion of the chromophore inside the cavity of the cyclic polysaccharide.[28]

The behavior of compound **3** in solution was also analyzed by means of ^{1}H-NMR spectroscopy in deuterated chloroform. The changes observed in the chemical shift of different signals in compound **3** when compared to the chemical shift of the same protons in the model compounds **9** and **10** (see Table S1†) indicated the presence of folded conformations of compound **3** in the studied medium. Thus, for example, two of the aromatic protons in the anthracene moiety in model **9** appear at 8.26 and 8.02 ppm whereas they are observed at 8.05 and 7.99 ppm, respectively, in compound **3**. Similarly, a downfield shift of the NH-sulfonamide signal from 5.42 ppm in **10** to 6.05 ppm in **3** is detected. In the case of the aromatic signals from the dansyl unit they are shifted from 8.51 and 8.40 ppm in **10** to 8.41 and 8.30 in **3**, for example. Also, and very notably, the anthracene-bounded CH_2 protons become non-equivalent in **3** and the multiplet containing the protons from the ethylenic spacer is significantly resolved in the bichromophoric compound, which is a clear proof of the prevalence of conformations with an increased rigidity in the bichromophoric compound. It is clear that folded conformations have to be even more predominant for compound **3** in polar solvents than in deuterated chloroform as the folding would reduce the exposure of the apolar regions of the compound to the unfavourable solvent.[8]

Biological studies with live cells

The biological applicability of the new pH probe compound **3** was investigated using RAW 264.7 mouse macrophage cells imaged by means of confocal laser scanning microscopy. The speed of internalization of compound **3** by the RAW 264.7 cells was initially investigated. RAW 264.7 cells were incubated with the probe for 30 min and 5 min, and the images obtained

 This journal is © The Royal Society of Chemistry 2015

Published on 19 June 2015. Downloaded by Freie Universitaet Berlin on 02/07/2015 14:49:49.

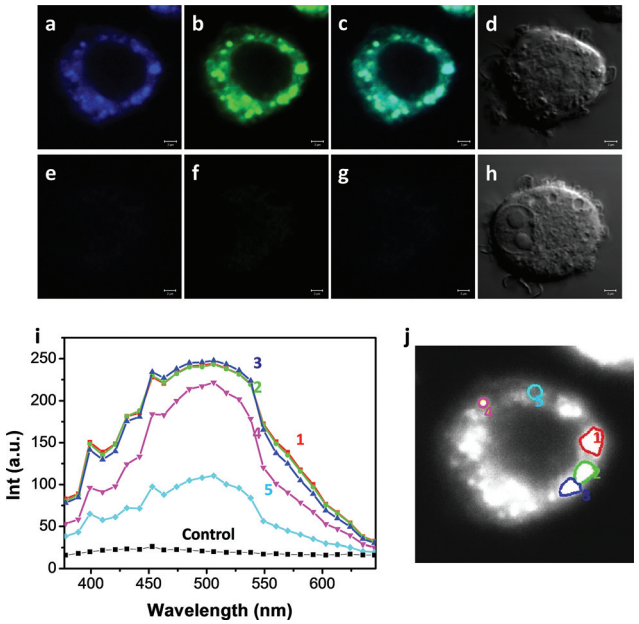

Fig. 5 Confocal microscopy images of RAW 264.7 cells: (a–d) loaded with compound **3** and (e–h) control cells without probe loaded. Fluorescence images collected in: (a and e) blue channel (380–430 nm, λ_{exc} = 364 nm), (b and f) green channel (470–500 nm, λ_{exc} = 364 nm), and (c and g) composite images of blue and green channels. (d and h) Differential interference contrast (DIC) images. Scale bars: 2 μm. (i) The fluorescence emission spectrum of the selected areas within a RAW 264.7 cell shown in (j) incubated with compound **3**. The fluorescence emission spectrum of a control cell is also shown in (i).

revealed a similar uptake (Fig. S19†). These experiments confirm the rapid internalization of compound **3** by the cells. For the remainder of the presented results, the 5 min incubation time was used. To collect the fluorescence emission of the two chromophores of compound **3**, the cells were excited with a 364 nm UV laser and the fluorescence emission was collected in the blue channel between 380 and 430 nm (to collect the emission due to the anthracene chromophore, Fig. 5a) and in the green channel between 470 and 500 nm (to collect the emission due to the dansyl chromophore, Fig. 5b). The images from the blue and the green channels coincide, indicating that both chromophores are together within the cell (Fig. 5c). DIC images of the RAW 264.7 cells (Fig. 5d) were collected simultaneously with the fluorescence images. Control experiments, without compound **3** loaded, were also performed using the same conditions (Fig. 5e–h). The internalization of compound **3** by the cells is clearly confirmed by the difference between the images obtained from the RAW 264.7 cells loaded with the probe and the images of control cells. To determine which of the fluorophores dominates within the cellular environment, the fluorescence emission spectrum of different regions within several RAW 264.7 cells was recorded (Fig. 5i and j, and Fig. S20 and S21†). The fluorescence emission intensity due to the dansyl chromophore (green channel, 470–500 nm) in compound **3** clearly dominates over the fluorescence emission intensity due to the anthracene chromophore (Fig. 5a, b, c and i). Although direct comparison of such spectra with those shown in Fig. 2 is not possible due to the different sensitivities of the detectors of the fluorimeter and the confocal microscope, it is clear that the EET process leading to emission of the dansyl fluorophore persists when the probe has been uptaken by the cell.

The typical PET pH probes based on amino protonation described in the literature are excellent markers of intracellular acidic organelles.[6a] Although compound **3** is a PET based probe, the acid–base analyses have confirmed that the fluorescence of this bichromophoric compound is enhanced with increasing values of pH and its pK_a was estimated to be 5.6. The acid–base behavior of **3** suggests that this compound should mark those organelles from within the cell whose pH is above *ca.* 5.6. In cells, the acidic organelles include the components of the endocytic pathway such as the early endosomes (pH range 6.0–6.5), late endosomes (pH range 5.0–6.0) and lysosomes (pH range 4.0–5.5). Therefore, compound **3** could mark some of the organelles included among the intracellular acidic organelles. Co-localization experiments using a selective marker for acidic organelles, LysoTracker Red DND-99,[29] were performed to determine the nature of the organelles marked by compound **3**. RAW 264.7 mouse macrophage cells were incubated with both DND-99 and compound **3** for 5 min. The fluorescence emission of compound **3** was collected in the blue (380–430 nm, Fig. 6a) and green (470–500 nm, Fig. 6b) channels after excitation of the cells with a 364 nm UV laser. The fluorescence emission of the LysoTracker Red DND-99 was collected above 560 nm (red channel, Fig. 6c) after excitation of the treated cells with a 543 helium–neon laser. As expected, Fig. 6 (and Fig. S22†) shows a perfect co-localization between the blue and green channels (due to the two fluorophores

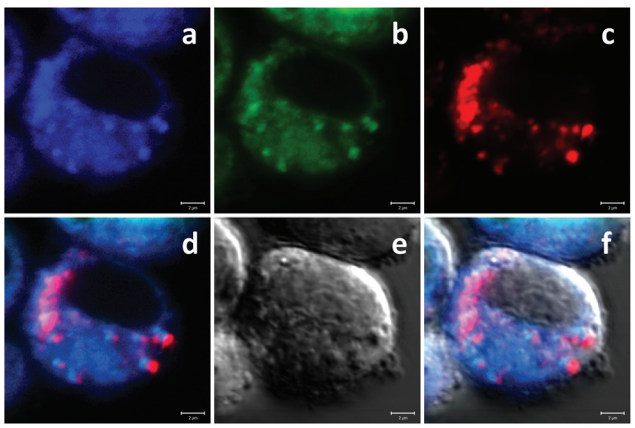

Fig. 6 Confocal fluorescence microscopy images of a RAW 264.7 cell loaded with compound **3** and LysoTracker Red DND-99. Fluorescence images correspond to the fluorescence emission due to: (a) anthracene chromophore in compound **3** (blue channel, 380–430 nm, λ_{exc} = 364 nm), (b) dansyl chromophore in compound **3** (green channel, 470–500 nm, λ_{exc} = 364 nm), (c) LysoTracker Red DND-99 (red channel, above 560 nm, λ_{exc} = 543 nm), (d) composite images of blue, green and red channels, (e) DIC image, and (f) composite image of blue, green and red channels and DIC. Scale bars: 2 μm.

Published on 19 June 2015. Downloaded by Freie Universitaet Berlin on 02/07/2015 14:49:49.

responsible for these emissions being together in compound **3**) and a partial co-localization between the blue and green channels with the red channel (emission due to the LysoTracker Red DND-99). A DIC image of the cell was obtained simultaneously with the three-channel fluorescence images (Fig. 6e). The overlay of the blue, green and red channels with the DIC image can be seen in Fig. 6f. The results obtained from the co-localization studies are in agreement with the expected behavior of compound **3**. A preliminary evaluation of the suitability of the probe as a ratiometric intracellular pH probe has been performed. Firstly, 18 different macrophage cells were sampled and areas within the macrophages that showed a high fluorescence intensity were selected. The fluorescence emission spectra of the bichromophoric probe from these specific areas were recorded using a confocal microscope. Using the calibration curve, Fig. 4, and the recorded spectra, the pH of 102 different regions within the 18 studied cells was estimated by determining the fluorescence intensity ratio of 496/421 nm and using the methodology previously described by Marín *et al.*[6e] The mean estimated pH value for these 102 different regions was determined to be between 5.4 and 5.9. These values are in agreement with the reported values of pH for the organelles of the endocytic pathway such as late endosomes and for lysosomes. Further, the fluorescence emission spectrum recorded from each of the 18 whole macrophage cells was also used to calculate the pH value reported by the bichromophoric probe. The values obtained for these whole macrophage cells ranged from 5.4 to 5.8. These combined data indicate that the bichromophoric probe is located within, and reports the pH of the acidic organelles of the analysed macrophage cells.

Experimental

Chemicals and starting materials

All commercially available reagents were used without further purification. *N*-Cbz-L-valine and *N*-Boc-ethylenediamine were purchased from Iris Biotech GmbH. *N*-Hydroxysuccinimide, DCC, tetrabutylammonium iodide (TBAI), 9-(chloromethyl)-anthracene, 1-pyrenecarboxylic acid, 4-chloro-7-nitrobenzo-2-oxo-1,3-diazole (NBD-Cl) and dansyl chloride (DNS-Cl) were commercially available from Fluka. Palladium, 5 wt% (dry basis) on activated carbon, water *ca.* 50% and thionyl chloride ($SOCl_2$), were obtained from Aldrich. Triethylamine (Et_3N), K_2CO_3, HCl (c), as well as the solvents were used as received from Scharlau. All chemicals were purchased in their highest purity grade. Solvents used for the spectrometric studies were of spectroscopic grade. Deuterated solvents were obtained from Euriso-top.

Biological studies

Dulbecco's Modified Eagle Medium (DMEM) (1×) containing 4.5 g L^{-1} D-glucose and phenol red as indicator, L-glutamine (200 mM), penicillin–streptomycin (100 U mL^{-1} and 100 μg mL^{-1}, respectively) and LysoTracker Red DND-99 (1 mM in DMSO) were purchased from Invitrogen. Fetal calf serum (FCS) was purchased from Biosera Ltd, UK. Nunc Easy flasks with porous caps, Nunc cryo tubes, 18 mm diameter glass coverslips and cryogenic freezing container were purchased from Thermo Fisher Scientific. Millex GP syringe driven filter units (0.22 μm) were purchased from Millipore Corporation, USA. Sterile centrifuge tubes and sterile disposable serological pipettes individually wrapped were purchased from Corning B. V. Life Sciences, The Netherlands. Cell scrapers (200 mm handle × 18 mm blade) were purchased from Fisher Scientific, UK.

RAW 264.7 mouse macrophages cells were purchased from ATCC. RAW 264.7 mouse macrophage cell line was kindly provided by Dr Jelena Gavrilovic (School of Biological Sciences, University of East Anglia, Norwich Research Park, Norwich, UK).

General methods

Nuclear magnetic resonance. Spectra were recorded using a Varian INOVA 500 spectrometer (500 MHz for ^{1}H-NMR and 125 MHz for ^{13}C-NMR) using deuterated solvents at room temperature unless otherwise indicated. Chemical shifts are reported in ppm using residual non-deuterated solvent peaks as internal standards.

Mass spectrometry. Mass spectra (ESI) were recorded using a Micromass Quatro LC spectrometer equipped with an electrospray ionization source and a triple-quadrupole analyzer. A QTOF Premier instrument with an orthogonal Z-spray-electrospray interface (Waters, Manchester, UK) was used operating in the W-mode. The drying and cone gas was nitrogen set to flow rates of 300 and 30 L h^{-1}, respectively. A capillary voltage of 3.5 kV was used in the positive scan mode, and the cone voltage was set to U_c = 10 V range. For accurate mass measurements, a 2 mg L^{-1} standard solution of leucine enkephalin was introduced *via* the lock spray needle at a cone voltage set to 85 V and a flow rate of 30 μL min^{-1}.

X-ray crystallography. Crystal data for **3** were collected on a SuperNova, Dual, Cu at zero, Atlas diffractometer. The crystal was kept at 293(2) K during data collection. A numerical absorption correction based on Gaussian integration over a multifaceted crystal model was applied using Olex2,[30] the structure was solved with the ShelXS[31] structure solution program using direct methods and refined with the ShelXL[31] refinement package using least squares minimization. These experiments were performed at the SCIC/UJI. Cambridge Crystallographic Data Centre CCDC 1057020 contains the supplementary crystallographic data for **3**.

IR spectroscopy. Attenuated total reflectance (ATR) FTIR spectra were acquired on a JASCO 6200 equipment with a MIRacle single-reflection ATR diamond/ZnSe accessory. The raw IR data were processed with the JASCO spectral manager software.

UV-visible and fluorescence spectroscopy. UV/Vis absorption spectra were recorded with a Hewlett–Packard 8453 spectrophotometer. Steady-state fluorescence spectra were acquired with a Spex Fluorolog 3-11 instrument equipped with a 450 W xenon lamp (right angle mode). All measurements were performed at 298 K unless otherwise indicated. The spectra were processed with the appropriate correction files.

 This journal is © The Royal Society of Chemistry 2015

Published on 19 June 2015. Downloaded by Freie Universitaet Berlin on 02/07/2015 14:49:49.

Time-resolved fluorescence measurements were performed by the time-correlated single-photon counting (TCSPC) technique with an IBH-5000U instrument. Samples were excited with a 372 nm NanoLED (pulse width 1.3 ns) at a repetition rate of 100 kHz. Data were fitted to an exponential model using eqn (6) after deconvolution of the instrument response function by an iterative deconvolution technique using the IBH DAS6 fluorescence decay analysis software in which reduced χ^2 (<1.2) and weighted residuals serve as parameters for goodness-of-fit measurements. All measurements were performed at 295 K (SCIC-UJI):

$$I(t) = \sum_i \alpha_i \exp\left(-\frac{t}{\tau_i}\right) \quad (6)$$

Fluorescence quantum yields (ϕ_F) of bichromophoric compound **3** and model compounds **9** and **10** in methanol and acidic methanol were determined using eqn (7):

$$\phi_F = \phi_{ref} \frac{A_{ref} F_s n_s^2}{A_s F_{ref} n_{ref}^2} \quad (7)$$

where A_s and A_{ref} are the absorbance of the sample and reference solutions, respectively, at the same excitation wavelength; F_s and F_{ref} are the corresponding relative integrated fluorescence intensities of the sample and reference; and n_s and n_{ref} are the average refractive indexes of the solvents used to measure the sample and the reference.

Synthesis and characterization of compounds

The synthetic route followed for the compounds reported is shown in Scheme 1 and is based on reported methods with some modifications.[8,32] The detailed procedures and the data obtained from the characterization of the compounds are described below. Compound **4** was synthesized as described previously.[8]

Synthesis of 5. The *N*-hydroxysuccinimide ester of *N*-Cbz-L-valine **4** (2.035 g, 5.84 mmol) was dissolved in anhydrous THF (150 mL) and cooled in an ice bath. *N*-Boc-ethylenediamine (0.945 g, 5.87 mmol) dissolved in dry THF (20 mL) was added slowly. The reaction mixture was stirred at room temperature for 18 h under a N_2 atmosphere. The reaction was followed by TLC using CH_2Cl_2 : MeOH (20 : 1) as the mobile phase. Then, the solvent was evaporated under reduced pressure and the reaction crude was purified by flash column chromatography on silica gel using CH_2Cl_2 : MeOH (40 : 1) as the eluent to yield a white solid (1.99 g, yield 87%). IR (ATR) 3333–3314 (complex, several bands), 3066, 2973, 1684, 1644, 1528, 1451, 1365, 1238 cm^{-1}. ^{1}H-NMR (500 MHz, $CDCl_3$) δ 7.44–7.28 (m, 5H), 6.66 (s, 1H), 5.41 (d, J = 6.4 Hz, 1H), 5.10 (dd, J = 24.4, 12.2 Hz, 2H), 4.97 (s, 1H), 4.04–3.90 (m, 1H), 3.35 (s, 2H), 3.25 (s, 2H), 2.12 (td, J = 13.2, 6.6 Hz, 1H), 1.43 (s, 9H), 0.93 (dd, J = 22.4, 6.8 Hz, 6H). ^{13}C-NMR (125 MHz, $CDCl_3$) δ 171.95, 156.94, 156.61, 136.40, 128.82, 128.52, 128.32, 128.17, 128.04, 79.89, 67.22, 60.65, 40.72, 40.35, 31.08, 28.57, 19.30, 17.85. ESI-MS (m/z): $(M + H)^+$ 394.4, $(M + Na)^+$ 416.3, $(M + K)^+$ 432.3.

Synthesis of 6. To a deoxygenated solution of **5** (1.95 g, 5 mmol) in MeOH (60 mL), Pd/C catalyst (palladium, 5 wt% (dry basis) on activated carbon, water *ca.* 50%) was added (200 mg). The mixture was then stirred for 8 h under a H_2 atmosphere (1 atm). The progress of the reaction was monitored by TLC and, finally, the reaction mixture was filtered over Celite to remove the catalyst and the filtered solution evaporated to dryness to afford **6** as a colourless oil (1.3 g, yield > 99.9%). IR (ATR) 3350–3300 (complex, several bands), 2969, 1686, 1651, 1527, 1453, 1365, 1249, 1167 cm^{-1}. ^{1}H-NMR (500 MHz, $CDCl_3$) δ 7.49 (s, 1H), 4.92 (s, 1H), 3.43–3.31 (m, 2H), 3.26 (dd, J = 11.1, 5.5 Hz, 2H), 3.21 (d, J = 3.9 Hz, 1H), 2.34–2.16 (m, 1H), 1.43 (s, 9H), 0.97 (t, J = 8.9 Hz, 3H), 0.83 (d, J = 6.9 Hz, 3H). ^{13}C-NMR (125 MHz, $CDCl_3$) δ 175.40, 156.57, 79.52, 60.38, 40.92, 39.64, 31.10, 28.46, 19.71, 16.23. ESI-MS (m/z): $(M + H)^+$ 260.

Synthesis of 7. Amine **6** (1.27 g, 4.92 mmol), dry K_2CO_3 (6.80 g, 49.2 mmol), tetrabutylammonium iodide (1.84 g, 4.92 mmol) and 9-(chloromethyl)anthracene (1.53 g, 4.92 mmol) were dissolved in dry CH_3CN (175 mL). The mixture was refluxed for 18 h under a N_2 atmosphere in the dark. The solution was then hot filtered to separate the insoluble K_2CO_3 and the solvent evaporated under reduced pressure. The crude product was redissolved in $CHCl_3$ (50 mL) and extracted with aqueous NaOH 0.01 M (4 × 50 mL). The organic phase was dried over anhydrous $MgSO_4$ and the solvent was evaporated under reduced pressure. The crude product was purified by silica flash chromatography using CH_2Cl_2 : MeOH (40 : 1) as the eluent to give **7** as a yellow solid (1.713 g, yield 77%). IR (ATR) 3339–3314 (complex, several bands), 3051, 2969, 1682, 1639, 1530, 1444, 1366, 1280, 1167 cm^{-1}. ^{1}H-NMR (500 MHz, $CDCl_3$) δ 8.41 (s, 1H), 8.26 (d, J = 8.9 Hz, 2H), 8.01 (d, J = 8.4 Hz, 2H), 7.64 (t, J = 5.7 Hz, 1H), 7.57 (dd, J = 8.1, 7.2 Hz, 2H), 7.50–7.44 (m, 2H), 5.05 (s, 1H), 4.66 (dd, J = 39.3, 12.5 Hz, 2H), 3.44 (pd, J = 13.2, 5.7 Hz, 2H), 3.29 (d, J = 4.9 Hz, 2H), 3.23 (d, J = 4.4 Hz, 1H), 2.13 (td, J = 13.3, 6.6 Hz, 1H), 1.41 (s, 9H), 0.97 (d, J = 6.9 Hz, 3H), 0.82 (d, J = 6.9 Hz, 3H). ^{13}C-NMR (125 MHz, $CDCl_3$) 174.92, 156.40, 131.70, 130.79, 130.32, 129.54, 129.49, 127.77, 127.72, 126.72, 126.59, 125.27, 125.15, 123.75, 79.53, 69.17, 45.63, 41.43, 39.26, 31.55, 28.55, 19.91, 17.80. ESI-MS (m/z): $(M + H)^+$ 450.4, $(M + Na)^+$ 472.4, $(2M + H)]^+$ 899.6, $(2M + Na)^+$ 921.5.

Synthesis of 8. Compound **7** (0.59 g, 1.31 mmol) dissolved in MeOH was cooled in an ice bath for 30 min under a N_2 atmosphere and a solution of HCl (c) (2.5 mL, 21 eq.) in MeOH (10 mL) was added. The reaction mixture was allowed to warm to room temperature and stirred for 18 h. Distilled water (20 mL) was added, followed by heating at 40 °C overnight. The methanolic solvent was evaporated under reduced pressure and the resulting mixture diluted with distilled water (25 mL). Then the acidic aqueous phase was extracted with $CHCl_3$ (3 × 50 mL). The aqueous layer was basified to pH 12 using NaOH 0.01 M, after which a yellowish precipitate appeared in the solution. This suspension was extracted with $CHCl_3$ (5 × 50 mL). The organic phase was dried over anhydrous $MgSO_4$ and the solvent was evaporated under reduced

Published on 19 June 2015. Downloaded by Freie Universitaet Berlin on 02/07/2015 14:49:49.

pressure to obtain **8** as a yellow solid (0.44 g, yield 97%). IR (ATR) 3296–3272 (complex, several bands), 3051, 2955, 1633, 1546, 1443, 1342 cm^{-1}. ^{1}H-NMR (500 MHz, $CDCl_3$) δ 8.33 (s, 1H), 8.24 (d, J = 8.9 Hz, 2H), 7.94 (d, J = 8.4 Hz, 2H), 7.61 (t, J = 5.5 Hz, 1H), 7.54–7.48 (m, 2H), 7.46–7.39 (m, 2H), 4.59 (dd, J = 52.7, 12.4 Hz, 2H), 3.39–3.28 (m, 2H), 3.20 (d, J = 4.6 Hz, 1H), 2.83–2.74 (m, 2H), 2.12 (tq, J = 13.5, 6.7 Hz, 1H), 1.70 (bs, 2H), 0.98 (d, J = 6.9 Hz, 3H), 0.80 (d, J = 6.9 Hz, 3H). ^{13}C-NMR (125 MHz, $CDCl_3$) δ 173.99, 131.44, 130.68, 130.09, 129.24, 129.21, 127.44, 126.24, 126.21, 124.93, 124.89, 123.66, 69.17, 45.48, 41.97, 41.77, 31.30, 19.74, 17.58. HRMS (ESI-TOF)$^+$ (m/z) calcd for $C_{39}H_{35}N_3O_2$ $(M + H)^+$ 350.2232, found 350.2228.

Synthesis of compound 1. 1-Pyrenecarboxylic acid (57.6 mg, 0.23 mmol) was allowed to react with an excess of thionyl chloride (6 mL) for 3 h under a N_2 atmosphere. The reaction mixture was distilled under vacuum to isolate the acyl chloride formed. A solution of amine **8** (80 mg, 0.23 mmol) in CH_2Cl_2 containing an excess of triethylamine (160 μL, 5 eq.) was added dropwise to this acyl chloride and the stirring was continued in the dark for 8 h. The resulting mixture was concentrated under reduced pressure and the residue was purified by flash column chromatography on silica gel using CH_2Cl_2 : MeOH (40 : 1) as the eluent to give the anthracene–dansyl dye **1** as a cream colored solid (54.6 mg, yield 41%). IR (ATR) 3290, 3051, 2957, 1643, 1628, 1600, 1524, 1444, 1218 cm^{-1}. ^{1}H-NMR (500 MHz, DMF-d_7) δ 8.64 (d, J = 9.3 Hz, 1H), 8.44 (d, J = 4.0 Hz, 2H), 8.42 (s, 1H), 8.28 (d, J = 7.8 Hz, 1H), 8.24 (d, J = 7.5 Hz, 1H), 8.21–8.16 (m, 3H), 8.13 (d, J = 9.0 Hz, 2H), 8.04 (t, J = 7.6 Hz, 1H), 8.00 (d, J = 8.4 Hz, 2H), 7.50–7.45 (m, 2H), 7.43–7.38 (m, 2H), 4.71 (d, J = 11.5 Hz, 1H), 4.55 (d, J = 12.6 Hz, 1H), 3.76 (d, J = 6.2 Hz, 2H), 3.70 (dd, J = 9.0, 6.5 Hz, 2H), 3.70 (td, J = 12.1, 6.1 Hz, 2H), 3.18 (d, J = 6.0 Hz, 1H), 1.95–1.87 (m, 1H), 0.89 (dd, J = 23.7, 6.7 Hz, 6H). HRMS (ESI-TOF)$^+$ (m/z) calcd for $C_{39}H_{35}N_3O_2$ $(M + H)^+$ 578.2808, found 578.2803. Absorption bands (λ, nm): 343–384 (neutral MeOH); 343–389 (acidic MeOH). Emission bands (λ, nm): 440 (neutral MeOH); 375–550 (acidic MeOH).

Synthesis of compound 2. To a solution of 4-chloro-7-nitrobenzo-2-oxo-1,3-diazole (86.6 mg, 0.43 mmol) in EtOH (6 mL), amine **8** (150 mg, 0.43 mmol) dissolved in EtOH (30 mL) was added dropwise over 20 min. The reaction mixture was stirred overnight at room temperature and a dark-green precipitate appeared as the reaction progressed. To ensure the completion of the reaction, this was refluxed for 5 h. The solvent was evaporated under vacuum and the residue was purified by flash column chromatography on silica gel using CH_2Cl_2 : MeOH (100 : 1) as the eluent to give the anthracene–dansyl dye **2** as an orange solid (170 mg, yield 77%). IR (ATR) 3307–3258 (complex, several bands), 3078, 2940, 1633, 1596, 1524, 1491, 1445, 1353, 1329, 1282, 1133 cm^{-1}. ^{1}H-NMR (500 MHz, DMSO-d_6) δ 9.31 (s, 1H), 8.50 (d, J = 7.8 Hz, 2H), 8.30 (d, J = 9.2 Hz, 2H), 8.23 (d, J = 5.2 Hz, 1H), 8.05 (dd, J = 6.9, 2.7 Hz, 2H), 7.59–7.39 (m, 4H), 6.51 (d, J = 9.0 Hz, 1H), 4.43 (dd, J = 49.3, 12.3 Hz, 2H), 3.65 (m, 2H), 3.54 (m, 2H), 3.03 (d, J = 5.6 Hz, 1H), 2.08 (s, 1H), 1.76 (dt, J = 13.3, 6.6 Hz, 1H), 0.80 (dd, J = 23.3, 6.7 Hz, 6H). ^{13}C-NMR (125 MHz, DMSO-d_6) δ 174.67, 145.23, 144.36, 137.80, 131.48, 131.00, 129.89, 128.78, 126.76, 125.88, 125.01, 124.32, 99.29, 67.96, 44.26, 43.43, 37.14, 31.05, 19.58, 18.39. HRMS (ESI-TOF)$^+$ (m/z) calcd for $C_{28}H_{28}N_6O_4$ $(M + H)^+$ 513.2250, found 513.2247. Absorption bands (λ, nm): 331–385 and 400–525 (neutral MeOH); 333–388 and 401–525 (acidic MeOH). Emission bands (λ, nm): 530 (neutral MeOH); 528 (acidic MeOH).

Synthesis of compound 3. Dansyl chloride (156.7 mg, 0.57 mmol) and triethylamine (200 μL, 2.5 eq.) were added to a solution of **8** (200 mg, 0.57 mmol) in CH_2Cl_2 (50 mL). The reaction mixture was stirred at room temperature for 24 h under a N_2 atmosphere. The resulting mixture was concentrated under reduced pressure and the residue was purified by flash column chromatography on silica gel using CH_2Cl_2 : MeOH (40 : 1) as the eluent to give the anthracene–dansyl dye **3** as a lime-green solid (247 mg, yield 74%). IR (ATR) 3310, 3134, 3059, 2951, 1656, 1574, 1523, 1455, 1327, 1147, 1090 cm^{-1}. ^{1}H-NMR (500 MHz, $CDCl_3$) δ 8.41 (dd, J = 8.5, 0.6 Hz, 1H), 8.39 (s, 1H), 8.30 (d, J = 8.6 Hz, 1H), 8.25 (d, J = 7.3 Hz, 1H), 8.05 (d, J = 9.2 Hz, 2H), 7.99 (dd, J = 6.2, 3.3 Hz, 2H), 7.62 (t, J = 6.0 Hz, 1H), 7.53–7.38 (m, 6H), 7.06 (d, J = 7.6 Hz, 1H), 6.05 (t, J = 4.9 Hz, 1H), 4.39 (dd, J = 64.1, 12.5 Hz, 2H), 3.50–3.35 (m, 1H), 3.34–3.23 (m, 1H), 3.19–3.08 (m, 2H), 3.02 (qd, J = 9.2, 4.7 Hz, 1H), 2.70 (s, 6H), 2.02 (td, J = 13.4, 6.7 Hz, 1H), 0.90 (d, J = 6.9 Hz, 3H), 0.68 (d, J = 6.9 Hz, 3H). ^{13}C-NMR (125 MHz, $CDCl_3$) δ 152.08, 134.76, 131.61, 130.55, 130.51, 130.21, 130.10, 129.74, 129.71, 129.49, 129.44, 128.63, 128.53, 127.81, 126.67, 126.57, 125.23, 125.12, 123.60, 123.56, 123.29, 123.18, 119.09, 115.33, 115.27, 68.72, 45.39, 45.34, 45.30, 44.51, 38.83, 31.22, 19.78, 17.65. HRMS (ESI-TOF)$^+$ (m/z) calcd for $C_{34}H_{38}N_4O_3S$ $(M + H)^+$ 583.2743, found 583.2744. Absorption bands (λ, nm): 331–385 (neutral MeOH); 334–388 (acidic MeOH). Emission bands (λ, nm): 519 (neutral MeOH); 375–450 (acidic MeOH).

Synthesis of model compound 9. This model compound was obtained as described above for compound **3**, starting from **8** and acetyl chloride. The crude product was purified by column chromatography on silica gel using CH_2Cl_2 : MeOH (16 : 1) as the eluent to give the anthracene–acetamide **9** as a yellow solid (38 mg, yield 51%). IR (ATR) 3312, 3064, 2956, 1626, 1550, 1446, 1371, 1280, 1115 cm^{-1}. ^{1}H-NMR (500 MHz, $CDCl_3$) δ 8.44 (s, 1H), 8.26 (d, J = 8.8 Hz, 2H), 8.02 (d, J = 8.3 Hz, 2H), 7.80 (bs, 1H), 7.58 (t, J = 7.1 Hz, 2H), 7.48 (t, J = 7.4 Hz, 2H), 6.53 (bs, 1H), 4.78 (s, 2H), 3.46–3.21 (m, 6H), 2.20 (qd, J = 19.5, 6.0 Hz, 1H), 1.89 (d, J = 2.2 Hz, 3H), 1.00–0.96 (m, 3H), 0.87 (d, J = 6.1 Hz, 3H). ^{13}C-NMR (125 MHz, $CDCl_3$) δ 170.84, 131.65, 130.41, 129.59, 128.17, 126.83, 125.28, 123.59, 68.76, 45.33, 41.09, 38.93, 31.24, 23.29, 19.65, 17.87. HRMS (ESI-TOF)$^+$ (m/z) calcd for $C_{24}H_{29}N_3O_2$ $(M + H)^+$ 392.2338, found 392.2333.

Synthesis of model compound 10. This compound was obtained as described above for compound **3** starting from *n*-propyl amine. The crude product was purified by column chromatography on silica gel using CH_2Cl_2 as the eluent to give the dansyl–propyl derivative **10** as a lime-green solid (210 mg, yield 95%). IR (ATR) 3281, 3054, 2960, 1580, 1435, 1312, 1144, 1076 cm^{-1}. ^{1}H-NMR (500 MHz, $CDCl_3$) δ 8.51

 This journal is © The Royal Society of Chemistry 2015

Published on 19 June 2015. Downloaded by Freie Universitaet Berlin on 02/07/2015 14:49:49.

(d, J = 8.5 Hz, 1H), 8.40 (d, J = 8.7 Hz, 1H), 8.25 (dd, J = 7.3, 1.2 Hz, 1H), 7.53–7.45 (m, 2H), 7.13 (d, J = 7.5 Hz, 1H), 5.42 (t, J = 6.1 Hz, 1H), 2.90–2.79 (m, 8H), 1.41–1.32 (m, 2H), 0.70 (t, J = 7.4 Hz, 3H). ^{13}C-NMR (125 MHz, $CDCl_3$) δ 152.71, 135.91, 130.97, 130.59, 130.43, 130.06, 129.04, 123.88, 123.84, 119.68, 115.83, 77.93, 77.68, 77.42, 45.65, 45.61, 45.32, 23.05, 11.09. HRMS (ESI-TOF)$^+$ (m/z) calcd for $C_{15}H_{20}N_2O_2S$ $(M + H)^+$ 293.1324, found 293.1325.

Spectroscopic studies

UV-visible and fluorescence measurements. Absorption and steady-state fluorescence measurements were performed dissolving the different compounds in spectroscopic grade MeOH, with a concentration of 3.8×10^{-5} M, 5.3×10^{-5} M and 3.9×10^{-5} M for bichromophoric compounds **1**, **2** and **3**, respectively, and 5.6×10^{-5} M and 5.0×10^{-5} M for model compounds **9** and **10**. The samples for fluorescence lifetime determination of compounds **3**, **9**, **10** were prepared from 1×10^{-3} M stock solutions in spectroscopic MeOH that were further diluted with MeOH to 1.7×10^{-5} M for compounds **3** and **9**, and to 2.5×10^{-5} M for compound **10**. Time-resolved fluorescence was measured using the TCSPC technique, as described above. The resulting emission was monitored at 420 nm for the study of the anthracene fraction, and at 550 nm in the case of the dansyl moiety, obtaining the corresponding decay curves. The recorded lifetimes ranged from 7.3 to 12.0 ns in the case of the model compounds and from 3.5 to 8.6 ns for bichromophoric compound **3**. Fluorescent quantum yields of compounds **3**, **9**, **10** are reported relative to quinine sulfate (aqueous solution, H_2SO_4 0.5 M, ϕ_F = 0.546).[33] Solutions of the compounds were prepared as described for the fluorescence lifetime determination. The experiments were performed using optically matching solutions upon excitation at the coincident absorption wavelength. Quartz fluorescence cuvettes (10 × 10 mm) were used in all cases. The lifetime of each compound was measured in neutral and in acidic methanol; the latter was achieved by addition of three drops of trifluoroacetic acid to the neutral sample (3 mL).

pH titration of compound 3. A stock solution of compound **3** (1×10^{-3} M) in DMSO (HPLC grade) was prepared and diluted with ultrapure Milli-Q® water. The pH titration was performed measuring the fluorescence emission of an aqueous solution of compound **3** (2×10^{-6} M, 0.2% DMSO) containing NaCl (0.1 M) at different pH values. pH modifications were achieved by addition of aliquots of aqueous NaOH and HCl solutions of different concentrations (0.05–1.00 M). The fluorescence emission was recorded between 380 and 650 nm, with excitation at 375 nm.

Biological studies

Imaging medium. The imaging medium based on Hank's balanced salt solution (HBSS) was prepared in water containing NaCl (120 mM), KCl (5 mM), $CaCl_2$ (2 mM), $MgCl_2$ (1 mM), $NaH_2PO_4{\cdot}2H_2O$ (1 mM), $NaHCO_3$ (1 mM) and 4-(2-hydroxyethyl)piperazine-4-ethanesulfonic acid (HEPES, 25 mM). The pH of the imaging medium was adjusted to pH 7.2. The imaging medium was supplemented with bovine serum albumin (1 mg mL^{-1}), basal medium eagle amino acids (2%), glutamine (2 mM) and glucose (11 mM). The imaging medium was sterilised by filtration through a Millex GP syringe driven filter unit (0.22 μm) prior to use.

Freezing RAW 264.7. To ensure the availability of a stock of the RAW 264.7 cell line, cells were grown, subcultured and stored in liquid nitrogen. The RAW 264.7 cells in a 75 cm^2 Nunc Easy Flasks cultured in DMEM containing 4.5 mg L^{-1} D-glucose and phenol red indicator and supplemented with 1% L-glutamine, 1% penicillin–streptomycin (100 U mL^{-1} and 100 μg mL^{-1}, respectively) and 10% FCS were harvested using a cell scraper (18 mm blade). The 12 mL of cells in supplemented DMEM were divided into four 75 cm^2 Nunc Easy Flasks (3 mL in each flask). Fresh supplemented DMEM (9 mL) was added to each flask. The cells were grown for 3 days in an incubator at 37 °C with a 5% CO_2 atmosphere. After 3 days of growth, the cells were harvested with a cell scraper. The content of each flask was transferred to a 15 mL sterile centrifuge tube and centrifuged at 1000 relative centrifugal force (rcf) for 5 min at 21 °C in an Eppendorf 5810R centrifuge. The supernatant containing old DMEM was removed and the pellet containing the RAW 264.7 cells was resuspended in 9.5 mL of freezing medium (90% supplemented DMEM and 10% culture grade DMSO). The cells in the freezing medium were placed in 1.8 mL Nunc cryo tubes (1 mL in each tube). The cryo tubes were placed in a cryogenic freezing container filled with propan-2-ol and were frozen to −80 °C overnight. The following day, the tubes were placed in a sample box and stored in liquid nitrogen for long term storage.

Passaging and subculturing RAW 264.7 cells. A cryo tube containing the RAW 264.7 cells (1 mL in freezing medium) was defrosted in a water bath at 37 °C. The cells were transferred to a 15 mL centrifuge tube containing fresh supplemented DMEM (9 mL). The suspension was centrifuged at 1000 rcf for 5 min at 21 °C in an Eppendorf 5810R centrifuge. The supernatant containing the freezing medium was removed and the cell pellet was resuspended in fresh supplemented DMEM (12 mL). The content of the centrifuge tube was transferred to a 75 cm^2 Nunc Easy flask and the flask was placed in an incubator at 37 °C under a 5% CO_2 atmosphere for 3 days. Subcultures (1 : 3) were made every three days by dislodging the cells from the flask surface using a cell scraper.

Culture of RAW 264.7 cells onto coverslips. For imaging, RAW 264.7 macrophage cells were cultured on 18 mm diameter glass coverslips 18–20 h prior to performing experiments. Cells were harvested from the Nunc Easy flask using an 18 mm blade cell scraper. A sterile coverslip was placed in each well in a 6-well Nunc multidish. Supplemented DMEM (2 mL) and an aliquot of the cell suspension (1 mL) were added to each well covering the coverslip. The cells were then incubated at 37 °C under a 5% CO_2 atmosphere overnight.

Incubation of RAW 264.7 macrophage cells with compound 3. The RAW 264.7 cells on the coverslip were loaded with **3** (50 μM, 0.25% DMSO) and incubated at 37 °C under a 5% CO_2 atmosphere for 30 min or for 5 min.

Published on 19 June 2015. Downloaded by Freie Universitaet Berlin on 02/07/2015 14:49:49.

Imaging of the RAW 264.7 macrophage cells incubated with compound 3. For imaging, coverslips containing the cells of interest were placed in a Ludin chamber (Life Imaging Service, Switzerland). Each coverslip was washed three times with imaging medium and the chamber mounted on a stage at 37 °C in a Carl Zeiss LSM510 META laser scanning confocal microscope. The cells were excited with a 364 nm UV laser. The fluorescence emission was measured between 380 and 430 nm for the blue channel (to collect the fluorescence emission due to the anthracene moiety) and between 470 and 500 nm for the green channel (to collect the fluorescence emission due to the dansyl moiety). Differential interference contrast (DIC) images were collected while simultaneously exciting the cells with a 488 nm argon-ion laser. All images were acquired with a plan-apochromat 63×, 1.4 NA oil-immersion objective. Fluorescence emission spectra of the samples were obtained using a lambda scan mode between 378 and 645 nm. The fluorescence emission intensity was measured in spectral bands each of 10.8 nm width.

Incubation of RAW 264.7 macrophage cells with compound 3 and LysoTracker Red DND-99. The RAW 264.7 cells on coverslips were loaded with **3** (50 μM, 0.25% DMSO) and LysoTracker Red DND-99 (2 μM, 0.2% DMSO) and incubated at 37 °C under a 5% CO_2 atmosphere for 5 min.

Imaging of the RAW 264.7 macrophage cells incubated with compound 3 and LysoTracker Red DND-99. For imaging, the cells were excited with a 364 nm UV laser to collect the fluorescence emission from compound **3**. The fluorescence emission was collected between 380 and 430 nm for the blue channel and between 470 and 500 nm for the green channel. To collect the fluorescence emission due to the LysoTracker Red DND-99, the cells were excited with a 543 nm helium–neon laser and the fluorescence emission was collected above 560 nm (red channel). Differential interference contrast (DIC) images were collected simultaneously using a 488 nm argon-ion laser as the excitation source. All images were acquired with a plan-apochromat 63×, 1.4 NA oil-immersion objective.

RAW 264.7 control cells. Images and fluorescence emission spectra of RAW 264.7 cells without dye loaded were obtained as described for RAW 264.7 cells loaded with compound **3**. These cells without compound **3** loaded were used as control experiments.

Conclusions

The three bichromophoric compounds prepared in this work (compounds **1–3**) containing an aminomethyl anthracene fragment and a second chromophore have been shown to experience EET processes from the anthracene moiety to the second chromophore. The X-ray structure of compound **3** revealed the folding characteristics of the pseudopeptidic spacer linking both subunits, a behavior described previously for other related pseudopeptides. The spectral behavior of these multifunctional compounds is modulated by a combination of PET and EET processes. Compound **3**, containing a dansyl as the second chromophore, displays the most interesting acid–base behavior. An off–on switching of the fluorescence associated with the dansyl fragment is observed when moving from an acidic environment to neutral–basic conditions upon excitation of the anthracene part. This behavior is considered to be opposite to that exhibited by related monochromophoric PET based systems. The pH titration curve of compound **3** is S-shaped instead of Z-shaped. Compound **3** offers a dual fluorescence response at two different spectroscopic regions, each affected by a different pH regulation. This fact, together with the possibility of ratiometric measurements, makes compound **3** a promising probe for biological studies. Preliminary studies using RAW 264.7 cells have shown that compound **3** is readily internalized by the cells and emits intracellularly in the green region mainly (470–500 nm). Co-localization studies with the LysoTracker Red DND-99 indicate a partial co-localization of the two probes. In addition a quantitative estimation of the pH by means of the corresponding calibration curve suggests that **3** could be marking organelles with acidic pH values between 5.4 and 5.8.

Acknowledgements

Financial support from the Spanish Ministerio de Economía y Competitividad (MINECO: CTQ2012-38543-C03-01), Generalitat Valenciana (PROMETEO/2012/020) and Universitat Jaume I (P1 1B2012-41) is acknowledged. V. S. thanks Universitat Jaume I for a PhD fellowship. Technical support by SCIC/UJI is also acknowledged. The authors are grateful for the financial support of the School of Chemistry, University of East Anglia, for M.J.M.

Notes and references

1 (*a*) H. Kobayashi, M. Ogawa, R. Alford, P. L. Choyke and Y. Urano, *Chem. Rev.*, 2009, **110**, 2620–2640; (*b*) K. Riehemann, S. W. Schneider, T. A. Luger, B. Godin, M. Ferrari and H. Fuchs, *Angew. Chem., Int. Ed.*, 2009, **48**, 872–897; (*c*) L. D. Lavis and R. T. Raines, *ACS Chem. Biol.*, 2008, **3**, 142–155; (*d*) Y. Yang, Q. Zhao, W. Feng and F. Li, *Chem. Rev.*, 2012, **113**, 192–270; (*e*) K. Saha, S. S. Agasti, C. Kim, X. Li and V. M. Rotello, *Chem. Rev.*, 2012, **112**, 2739–2779; (*f*) N. Johnsson and K. Johnsson, *ACS Chem. Biol.*, 2007, **2**, 31–38.

2 (*a*) L. Yuan, W. Lin, K. Zheng, L. He and W. Huang, *Chem. Soc. Rev.*, 2013, **42**, 622–661; (*b*) S. Wang, N. Li, W. Pan and B. Tang, *TrAC, Trends Anal. Chem.*, 2012, **39**, 3–37; (*c*) T. Doussineau, A. Schulz, A. Lapresta-Fernandez, A. Moro, S. Körsten, S. Trupp and G. J. Mohr, *Chem. – Eur. J.*, 2010, **16**, 10290–10299; (*d*) M. Y. Berezin and S. Achilefu, *Chem. Rev.*, 2010, **110**, 2641–2684; (*e*) S. M. Borisov and O. S. Wolfbeis, *Chem. Rev.*, 2008, **108**, 423–461; (*f*) A. Louie, *Chem. Rev.*, 2010, **110**, 3146–3195.

 This journal is © The Royal Society of Chemistry 2015

Published on 19 June 2015. Downloaded by Freie Universitaet Berlin on 02/07/2015 14:49:49.

3 (*a*) J. Han and K. Burgess, *Chem. Rev.*, 2009, **110**, 2709–2728; (*b*) Z. Liu, C. Zhang, W. He, F. Qian, X. Yang, X. Gao and Z. Guo, *New J. Chem.*, 2010, **34**, 656–660; (*c*) J. R. Casey, S. Grinstein and J. Orlowski, *Nat. Rev. Mol. Cell Biol.*, 2010, **11**, 50–61; (*d*) R. Pal and D. Parker, *Org. Biomol. Chem.*, 2008, **6**, 1020–1033; (*e*) D. G. Smith, B. K. McMahon, R. Pal and D. Parker, *Chem. Commun.*, 2012, **48**, 8520–8522; (*f*) X. Wan and S. Liu, *J. Mater. Chem.*, 2011, **21**, 10321–10329; (*g*) D. Wencel, T. Abel and C. McDonagh, *Anal. Chem.*, 2013, **86**, 15–29; (*h*) C. Thivierge, J. Han, R. M. Jenkins and K. Burgess, *J. Org. Chem.*, 2011, **76**, 5219–5228; (*i*) R. Wang, C. Yu, F. Yu and L. Chen, *TrAC, Trends Anal. Chem.*, 2010, **29**, 1004–1013; (*j*) Y. Ni and J. Wu, *Org. Biomol. Chem.*, 2014, **12**, 3774–3791; (*k*) F. Doria, M. Folini, V. Grande, G. Cimino-Reale, N. Zaffaroni and M. Freccero, *Org. Biomol. Chem.*, 2015, **13**, 570–576; (*l*) R. Søndergaard, J. R. Henriksen and T. L. Andresen, *Nat. Protoc.*, 2014, **9**, 2841–2858.

4 (*a*) B. Daly, J. Ling and A. P. de Silva, *Chem. Soc. Rev.*, 2015, DOI: 10.1039/C4CS00334A; (*b*) A. P. de Silva, T. S. Moody and G. D. Wright, *Analyst*, 2009, **134**, 2385–2393; (*c*) A. P. de Silva, H. Q. N. Gunaratne, T. Gunnlaugsson, A. J. M. Huxley, C. P. McCoy, J. T. Rademacher and T. E. Rice, *Chem. Rev.*, 1997, **97**, 1515–1566; (*d*) A. P. de Silva and S. Uchiyama, *Top. Curr. Chem.*, 2011, **300**, 1–28; (*e*) M. I. Burguete, F. Galindo, M. A. Izquierdo, S. V. Luis and L. Vigara, *Tetrahedron*, 2007, **63**, 9493–9501; (*f*) F. Galindo, J. Becerril, M. I. Burguete, S. V. Luis and L. Vigara, *Tetrahedron Lett.*, 2004, **45**, 1659–1662; (*g*) M. I. Burguete, F. Galindo, S. V. Luis and L. Vigara, *J. Photochem. Photobiol., A*, 2010, **209**, 61–67.

5 (*a*) H. M. Kim, M. J. An, J. H. Hong, B. H. Jeong, O. Kwon, J.-Y. Hyon, S.-C. Hong, K. J. Lee and B. R. Cho, *Angew. Chem., Int. Ed.*, 2008, **47**, 2231–2234; (*b*) A. P. de Silva and R. A. D. D. Rupasinghe, *J. Chem. Soc., Chem. Commun.*, 1985, 1669–1670; (*c*) J. C. Beeson, M. E. Huston, D. A. Pollard, T. K. Venkatachalam and A. W. Czarnik, *J. Fluoresc.*, 1993, **3**, 65–68; (*d*) J. F. Callan, A. P. de Silva, J. Ferguson, A. J. M. Huxley and A. M. O'Brien, *Tetrahedron*, 2004, **60**, 11125–11131; (*e*) S. Zheng, P. L. M. Lynch, T. E. Rice, T. S. Moody, H. Q. N. Gunaratne and A. P. de Silva, *Photochem. Photobiol. Sci.*, 2012, **11**, 1675–1681; (*f*) G. Greiner and I. Maier, *J. Chem. Soc., Perkin Trans. 2*, 2002, 1005–1011.

6 (*a*) F. Galindo, M. I. Burguete, L. Vigara, S. V. Luis, N. Kabir, J. Gavrilovic and D. A. Russell, *Angew. Chem., Int. Ed.*, 2005, **44**, 6504–6508; (*b*) M. I. Burguete, F. Galindo, M. A. Izquierdo, J.-E. O'Connor, G. Herrera, S. V. Luis and L. Vigara, *Eur. J. Org. Chem.*, 2010, 5967–5979; (*c*) P. D. Wadhavane, M. A. Izquierdo, D. Lutters, M. I. Burguete, M. J. Marín, D. A. Russell, F. Galindo and S. V. Luis, *Org. Biomol. Chem.*, 2014, **12**, 823–831; (*d*) M. J. Marín, F. Galindo, P. Thomas, T. Wileman and D. A. Russell, *Anal. Bioanal. Chem.*, 2013, **405**, 6197–6207; (*e*) M. J. Marín, F. Galindo, P. Thomas and D. A. Russell, *Angew. Chem., Int. Ed.*, 2012, **51**, 9657–9661.

7 (*a*) J. Liu, Z. Diwu and D. H. Klaubert, *Bioorg. Med. Chem. Lett.*, 1997, **7**, 3069–3072; (*b*) B. M. Weidgans, C. Krause, I. Klimant and O. S. Wolfbeis, *Analyst*, 2004, **129**, 645–650; (*c*) K. P. McNamara, T. Nguyen, G. Dumitrascu, J. Ji, N. Rosenzweig and Z. Rosenzweig, *Anal. Chem.*, 2001, **73**, 3240–3246; (*d*) C. R. Schroder, B. M. Weidgans and I. Klimant, *Analyst*, 2005, **130**, 907–916.

8 J. Becerril, M. Bolte, M. I. Burguete, F. Galindo, E. García-España, S. V. Luis and J. F. Miravet, *J. Am. Chem. Soc.*, 2003, **125**, 6677–6686.

9 J. Becerril, M. Bolte, M. I. Burguete, J. Escorihuela, F. Galindo and S. V. Luis, *CrystEngComm*, 2010, **12**, 1722–1725.

10 (*a*) S. Alvarez, *Dalton Trans.*, 2013, **42**, 8617–8636; (*b*) N. G. White, C. J. Serpell and P. D. Beer, *Cryst. Growth Des.*, 2014, **14**, 3472–3479.

11 I. Dance, *New J. Chem.*, 2003, **27**, 22–27.

12 J. R. Lakowicz, *Principles of Fluorescence Spectroscopy*, Springer Science+Business Media, New York, NY, 3rd edn, 2006.

13 N. J. Turro, *Modern molecular photochemistry*, University Science Books, Corp., Sausalito, CA, 1st edn, 1991.

14 (*a*) J.-P. Desvergne, A. Castellan and H. Bouas-Laurent, *Tetrahedron Lett.*, 1981, **22**, 3529–3532; (*b*) J. P. Desvergne, N. Bitit, A. Castellan, H. Bouas-Laurent and J. C. Soulignac, *J. Lumin.*, 1987, **37**, 175–181.

15 J. Zhou, X. Yuan, M. Jiang and Y. Zhang, *Macromol. Rapid Commun.*, 2000, **21**, 579–582.

16 B. Maubert, N. D. McClenaghan, M. T. Indelli and S. Campagna, *J. Phys. Chem. A*, 2003, **107**, 447–455.

17 J. Rohacova, M. L. Marín and M. A. Miranda, *J. Phys. Chem. B*, 2010, **114**, 4710–4716.

18 S. Banthia and A. Samanta, *J. Phys. Chem. B*, 2006, **110**, 6437–6440.

19 M. Gómez-Mendoza, M. L. Marín and M. A. Miranda, *J. Phys. Chem. B*, 2012, **116**, 14776–14780.

20 (*a*) B. Branchi, P. Ceroni, V. Balzani, M. C. Cartagena, F.-G. Klarner, T. Schrader and F. Vogtle, *New J. Chem.*, 2009, **33**, 397–407; (*b*) B. Branchi, P. Ceroni, V. Balzani, G. Bergamini, F.-G. Klärner and F. Vögtle, *Chem. – Eur. J.*, 2009, **15**, 7876–7882; (*c*) B. Branchi, P. Ceroni, V. Balzani, F.-G. Klärner and F. Vögtle, *Chem. – Eur. J.*, 2010, **16**, 6048–6055.

21 K. Kaur and S. Kumar, *Dalton Trans.*, 2011, **40**, 2451–2458.

22 (*a*) J. Andreasson and U. Pischel, *Chem. Soc. Rev.*, 2010, **39**, 174–188; (*b*) R. Ferreira, P. Remón and U. Pischel, *J. Phys. Chem. C*, 2009, **113**, 5805–5811; (*c*) P. P. Lima, S. S. Nobre, R. O. Freire, S. A. Júnior, R. A. Sá Ferreira, U. Pischel, O. L. Malta and L. D. Carlos, *J. Phys. Chem. C*, 2007, **111**, 17627–17634; (*d*) S. Abad, M. Kluciar, M. A. Miranda and U. Pischel, *J. Org. Chem.*, 2005, **70**, 10565–10568; (*e*) S. Abad, U. Pischel and M. A. Miranda, *J. Phys. Chem. A*, 2005, **109**, 2711–2717; (*f*) S. Abad, U. Pischel and M. A. Miranda, *Photochem. Photobiol. Sci.*, 2005, **4**, 69–74; (*g*) P. Remón, R. Ferreira, J.-M. Montenegro, R. Suau,

Published on 19 June 2015. Downloaded by Freie Universitaet Berlin on 02/07/2015 14:49:49.

E. Pérez-Inestrosa and U. Pischel, *ChemPhysChem*, 2009, **10**, 2004–2007.
23 P. Ceroni, I. Laghi, M. Maestri, V. Balzani, S. Gestermann, M. Gorka and F. Vogtle, *New J. Chem.*, 2002, **26**, 66–75.
24 S. L. Murov, I. Carmichael and G. L. Hug, *Handbook of Photochemistry*, Taylor & Francis, 2nd edn, 1993.
25 N. A. O'Connor, S. T. Sakata, H. Zhu and K. J. Shea, *Org. Lett.*, 2006, **8**, 1581–1584.
26 S. R. Holmes-Farley and G. M. Whitesides, *Langmuir*, 1986, **2**, 266–281.
27 (*a*) C. Schmuck and J. Dudaczek, *Eur. J. Org. Chem.*, 2007, 3326–3330; (*b*) H. Tamiaki and K. Maruyama, *J. Chem. Soc., Perkin Trans. 1*, 1992, 2431–2435; (*c*) S. V. Luis and I. Alfonso, *Acc. Chem. Res.*, 2014, **47**, 112–124.
28 R. Corradini, A. Dossena, G. Galaverna, R. Marchelli, A. Panagia and G. Sartor, *J. Org. Chem.*, 1997, **62**, 6283–6289.
29 S. D. Desai, R. E. Reed, S. Babu and E. A. Lorio, *J. Biol. Chem.*, 2013, **288**, 2388–2402.
30 O. V. Dolomanov, L. J. Bourhis, R. J. Gildea, J. A. K. Howard and H. Puschmann, *J. Appl. Crystallogr.*, 2009, **42**, 339–341.
31 G. M. Sheldrick, *Acta Crystallogr., Sect. A: Fundam. Crystallogr.*, 2008, **64**, 112–122.
32 (*a*) J. H. Cho, F. Amblard, S. J. Coats and R. F. Schinazi, *Tetrahedron*, 2011, **67**, 5487–5493; (*b*) Y. Kitano, Y. Nogata, K. Matsumura, E. Yoshimura, K. Chiba, M. Tada and I. Sakaguchi, *Tetrahedron*, 2005, **61**, 9969–9973; (*c*) J. F. Callan, A. P. de Silva, J. Ferguson, A. J. M. Huxley and A. M. O'Brien, *Tetrahedron*, 2004, **60**, 11125–11131; (*d*) A. Chouai, V. J. Venditto and E. E. Simanek, *Org. Synth.*, 2009, **86**, 141–150.
33 D. F. Eaton, *Pure Appl. Chem.*, 1988, **60**, 1107–1114.

 This journal is © The Royal Society of Chemistry 2015